

Quasiparticle self-consistent GW method based on the augmented plane-wave and muffin-tin orbital method

Takao Kotani

Department of applied mathematics and physics, Tottori university, Tottori 680-8552, Japan

(Dated: April 11, 2014)

We have developed the quasiparticle self-consistent *GW* (QSGW) method based on a recently developed mixed basis all-electron full-potential method (the PMT method), which uses the augmented plane waves (APWs) and the highly localized muffin-tin orbitals (MTOs) simultaneously. We call this PMT-QSGW. Because of the two kinds of augmented bases, we have efficient description of one-particle eigenfunctions in materials with small number of basis functions. In QSGW, we have to treat a static non-local exchange-correlation potential, which is generated from the self-energy. We expand the potential in the highly localized MTOs. This allows us to make stable interpolation of the self-energy in the whole Brillouin zone. In addition, we have improved the offset- Γ method for the Brillouin zone integration, so that we take into account the anisotropy of the screened Coulomb interaction in the calculation of the self-energy. For GaAs and cubic SiO₂, we checked convergence of calculated band gaps on cutoff parameters. PMT-QSGW is implemented in a first-principles electronic structure package `ecalj`, which is freely available from github.

PACS numbers: 71.15.Ap, 71.15.-m, 31.15.-p

I. INTRODUCTION

The quasiparticle self-consistent *GW* method (QSGW) is a self-consistent perturbation method within the *GW* approximation. QSGW find out an optimum static one-body Hamiltonian \hat{H}^0 describing the independent-particle picture (or the quasiparticle (QP) picture). In other words, QSGW divides the full many-body Hamiltonian \hat{H} into $\hat{H} = \hat{H}^0 + (\hat{H} - \hat{H}^0)$. Then $(\hat{H} - \hat{H}^0)$ is chosen so that it virtually does not affect to the determination of QPs. That is, we extract \hat{H}^0 as a kernel of \hat{H} . Note that $(\hat{H} - \hat{H}^0)$ should contain not only the bare Coulomb interaction but also quadratic term, which is missing in usual model Hamiltonians. Since we evaluate $(\hat{H} - \hat{H}^0)$ in the *GW* approximation in QSGW, we determine \hat{H}^0 (or the QPs, equivalently) with taking into account the charge fluctuation in the random phase approximation (RPA) self-consistently. QSGW is conceptually completely different from the fully self-consistent *GW* method¹⁻⁵, which tries to calculate the full one-body Green's function self-consistently.

QSGW was first introduced by Faleev, van Schilf-gaarde, and Kotani⁶. It was implemented based on the all-electron full-potential linearized muffin-tin orbital (FP-LMTO) package⁷ organized by van Schilf-gaarde, in combination with the *GW* package developed by Kotani initially for Ref.8, where he starts from a detailed analysis of a *GW* package developed by Aryasetiawan⁹⁻¹¹ based on the LMTO in the atomic sphere approximation. We refer to the implementation as FP-LMTO-QSGW in the followings. QSGW is now widely accepted as a possible candidate to go beyond limitations of current first-principles methods^{12,13} (we recently found that FP-LMTO-QSGW is taken to be for massively parallelized¹⁴). QSGW is also implemented in other first-principles electronic structure packages in different manners¹⁵⁻²⁰. For example, Bruneval have calcu-

lated ionization energies of atoms in QSGW^{18,19}.

In QSGW, we have to treat a static non-local exchange-correlation potential $V^{xc}(\mathbf{r}, \mathbf{r}')$ (spin index is omitted for simplicity here). It is given by removing the energy-dependence from the self-energy $\Sigma(\mathbf{r}, \mathbf{r}', \omega)$ in a manner (See Eq. (7)). We determine eigenvalues and eigenfunctions with $V^{xc}(\mathbf{r}, \mathbf{r}')$, with which we evaluate not only the diagonal, but also the off-diagonal elements. The importance of the off-diagonal elements is seen especially in the dispersion crossing. We see the (conventional) one-shot *GW* only with the diagonal self-energy can not give a band gap for Ge as shown Fig.6 in Ref.21. This is because the connectivity of the dispersion in GGA/LDA can not be altered. In contrast to the case, the connectivity is correctly altered when we include the off-diagonal elements (or fully include the non-locality).

To plot the energy-band dispersion in the whole Brillouin zone (BZ), we have to know non-local potential $V_{\mathbf{k}}^{xc}(\mathbf{r}, \mathbf{r}')$ at any \mathbf{k} point in the BZ by an interpolation, where \mathbf{r} and \mathbf{r}' are within the primitive cell. This interpolation is also needed for the offset- Γ method in Sec.III B, and useful for calculating physical quantities which requires integrations in the BZ. For the interpolation, we inevitably require real-space representation $V^{xc}(\mathbf{r}, \mathbf{R}' + \mathbf{r}')$, where \mathbf{R}' is to specify origin of primitive cells. If it is inverse Fourier transformed, we obtain $V_{\mathbf{k}}^{xc}(\mathbf{r}, \mathbf{r}')$ at any \mathbf{k} . The nature that the MTOs are atom-centered and localized basis enables us to make such an interpolation in FP-LMTO-QSGW²².

Even though FP-LMTO-QSGW have been successfully applied to many cases, e.g.,²³⁻²⁸, it still has problems. A main problem originates from the FP-LMTO method, the applicability of which is limited to the systems that can be described only by the MTOs. Because of this fact, we have to fill empty regions with empty spheres (ESs) in, e.g., not closed packed systems and surfaces. The effort of this procedure enforces us to repeat many calculations to

check numerical convergence. Therefore, it was not easy to apply QSGW to, e.g., surfaces. In addition, it is not so easy to enlarge basis set systematically as in the case of the LAPW method. Furthermore, the interpolation of $V_{\mathbf{k}}^{\text{xc}}(\mathbf{r}, \mathbf{r}')$ was unstable in cases because we needed to use not well-localized MTOs (they contain damping factor $\propto \exp(-r/\kappa)$ where $\kappa^{-2} \sim 0.1$ Ry. Thus the MTOs has long range). This required us to use a very complicated interpolation procedure²².

To overcome the problem in the FP-LMTO in DFT, we recently have given a new all-electron full-potential first-principles method of the electronic structure calculations in the GGA/LDA (one-body problem solver)^{29,30}. This method is named the linearized augmented plane wave and muffin-tin orbital method (the PMT method), which is a mixed basis method of augmented waves, the APWs and the MTOs. Within our knowledge, there is no other mixed-basis method of augmented waves. We can use a procedure to set parameters of the MTOs almost automatically as given in Ref.30. (see Fig.1 and Table.I around in Ref.30). The important point is that a serious difficulty in the FP-LMTO, how to set the parameters, is now overcome. In the usual FP-LMTO, we need to repeat many calculations to figure out reasonable parameters of the MTOs. In contrast, we can check convergence only by changing number of APWs. Based on the procedure, we find that the highly localized MTOs ($\kappa^{-2} = 1 \sim 2$ (bohr)⁻²) in combination with APWs whose cutoff energy ~ 4 Ry can give good convergence of total energy in the GGA/LDA³⁰; we successfully obtained atomization energy for homo-nuclear diatomic molecules, which is converged more than chemical accuracy (~ 1 Kcal/mol). Thus we can expand eigenfunctions with highly localized atom-centered MTOs and low energy APWs.

In this paper, we show how to implement the QSGW method in the PMT method, that is, the PMT-QSGW method. After we explain the QSGW theory in Sec. II, we explain the implementation of PMT-QSGW in Sec. III. Especially, in Sec. IIIB, we show new improvement to the offset- Γ method to take into the anisotropy of the screened Coulomb interaction accurately; in Sec. IIIC, we explain the interpolation of $V_{\mathbf{k}}^{\text{xc}}(\mathbf{r}, \mathbf{r}')$. Finally, in Sec.IV, we show detailed numerical tests for the band gap (at Γ point) for GaAs and cubic SiO₂ (β -cristobalite). We show how the QSGW band gap can depends on the cutoff parameters.

II. THEORY OF THE QSGW METHOD

Here we summarize the QSGW method. We treat the following many-body Hamiltonian for electronic system. With the field operators $\hat{\psi}_{\sigma}(\mathbf{r})$, spin index σ , external potential $V_{\sigma}^{\text{ext}}(\mathbf{r})$, and the Coulomb interaction $v(\mathbf{r}, \mathbf{r}') =$

$\frac{e^2}{|\mathbf{r}-\mathbf{r}'|}$, it is written as

$$\hat{H} = \hat{H}^{\text{k}} + \hat{V}^{\text{ee}} + \hat{V}^{\text{ext}}, \quad (1)$$

$$\hat{H}^{\text{k}} = \sum_{\sigma} \int d\mathbf{r} \hat{\psi}_{\sigma}^{\dagger}(\mathbf{r}) \left(-\frac{\nabla^2}{2m}\right) \hat{\psi}_{\sigma}(\mathbf{r}), \quad (2)$$

$$\hat{V}^{\text{ext}} = \sum_{\sigma} \int d\mathbf{r} V_{\sigma}^{\text{ext}}(\mathbf{r}) \hat{n}_{\sigma}(\mathbf{r}), \quad (3)$$

$$\hat{V}^{\text{ee}} = \frac{e^2}{2} \sum_{\sigma\sigma'} \int d^3r d^3r' v(\mathbf{r}, \mathbf{r}') \hat{\psi}_{\sigma}^{\dagger}(\mathbf{r}) \hat{\psi}_{\sigma'}^{\dagger}(\mathbf{r}') \hat{\psi}_{\sigma'}(\mathbf{r}') \hat{\psi}_{\sigma}(\mathbf{r}). \quad (4)$$

Here, we omit classical electrostatic nucleus-nucleus energy for simplicity. We explicitly show electron mass m and charge e^2 in the following formulas but with $\hbar = 1$. $V^{\text{ext}}(\mathbf{r})$ mainly contains those coming from nucleuses, in addition to perturbation such as external magnetic fields. Hats on symbols mean the second quantized quantities (for example, \hat{V}^{ext} and $V_{\sigma}^{\text{ext}}(\mathbf{r})$ mean the same physical quantities in different representations). In the followings, we omit the spin index σ and often \mathbf{r} for simplicity.

Let us consider how to obtain best one-body Hamiltonian H^0 to describe QPs for given \hat{H} . If we have the self-energy $\Sigma(\mathbf{r}, \mathbf{r}', \omega)$ for given \hat{H} , we can determine the QP energies and eigenfunctions as the solutions of

$$H(\epsilon_i) |\Psi_i(\mathbf{r})\rangle = \epsilon_i |\Psi_i(\mathbf{r})\rangle, \quad (5)$$

at least near the Fermi energy, where the one-particle dynamical effective Hamiltonian $H(\omega)$ is

$$H(\omega) = -\frac{\nabla^2}{2m} + V^{\text{ext}} + V^{\text{H}} + \Sigma(\omega). \quad (6)$$

Here V^{ext} is the external potential from nucleus and V^{H} is the Hartree potential. If $H(\omega)$ were ω -independent and Hermitian, we could have directly identified this as H^0 . Apparently this is not true, however, based on the Landau-Silin's QP theory (or the independent-particle picture), we can still expect that physical properties can be evaluated with the use of the eigenvalues and eigenfunctions of the QPs $\{\epsilon_i, \Psi_i(\mathbf{r})\}$. This means a physical picture that primary excitations are specified by electrons or holes added to these orbitals, then they interact each other with a screened Coulomb interaction. A theoretical inconvenience is that the set of QPs is not a complete set since $\Sigma(\omega)$ is energy-dependent non-Hermitian. If we can use a static Hermitian one-body potential $V^{\text{xc}}(\mathbf{r}, \mathbf{r}')$ in place of $\Sigma(\omega)$, such a problem does not occur. Then the set $\{\Psi_i(\mathbf{r})\}$ is an orthonormal complete set, and physical quantities can be represented in the Fock space of the set. In other words, we divide the full many-body Hamiltonian \hat{H} into $\hat{H} = \hat{H}^0 + (\hat{H} - \hat{H}^0)$, where the many-body contribution due to $(\hat{H} - \hat{H}^0)$, should not change the QPs given by \hat{H}^0 .

Following the above discussion, we need two methods to obtain such \hat{H}^0 for given \hat{H} . These are

- (i) A method to calculate $\Sigma(\omega)$ (and also V^{H}) for given division of $\hat{H} = \hat{H}^0 + (\hat{H} - \hat{H}^0)$.

- (ii) A method to determine V^{xc} as a good substitution of given $\Sigma(\omega)$.

If both methods (i) and (ii) are given, we can make a self-consistent cycle closed. That is, we have the cycle $\hat{H}^0 \rightarrow \{V^{\text{H}}, \Sigma(\omega)\} \rightarrow \hat{H}^0 \rightarrow \dots$. This is repeated until converged. In QSGW, we use the GW approximation for (i). As for (ii), we use a mapping from $\Sigma(\omega)$ to a static Hermitian potential $V^{\text{xc}}(\mathbf{r}, \mathbf{r}')$ as

$$\begin{aligned} V^{\text{xc}} &= \frac{1}{2} \int_{-\infty}^{\infty} d\omega \mathcal{R}[\Sigma(\omega)] \delta(\omega - H^0) + \text{c.c.} \\ &= \sum_{ij} |\Psi_i\rangle \langle \Psi_i| \frac{\mathcal{R}[\Sigma(\varepsilon_i) + \Sigma(\varepsilon_j)]}{2} |\Psi_j\rangle \langle \Psi_j|, \end{aligned} \quad (7)$$

where $\mathcal{R}[X] = \frac{X+X^\dagger}{2}$ means taking the Hermitian part of X . Eq. (7) is given so as to reproduce $\{\varepsilon_i, \Psi_i(\mathbf{r})\}$ satisfying Eq. (5) as good as possible (this is not a unique choice²²). If necessary, we can derive Eq. (7) from a minimization of the difference $G^{-1} - (G^0)^{-1}$, written as $\text{Tr}[(G^{-1} - (G^0)^{-1}) \delta((G^0)^{-1}) (G^{-1} - (G^0)^{-1})] + \text{c.c.}$ ¹². The GW approximation together with Eq. (7) makes a fundamental equation of QSGW.

Let us detail steps of the QSGW calculation. We start from a trial one-particle static Hamiltonian written as

$$H^0 = \frac{-\nabla^2}{2m} + V^{\text{eff}}(\mathbf{r}, \mathbf{r}'). \quad (8)$$

This H^0 is just the initial condition for iteration cycle, and does not affect the final result. The GW method is applied to the division $\hat{H} = \hat{H}^0 + (\hat{H} - \hat{H}^0)$. Its steps are as follows, (I)-(V).

- (I) We have the non-interacting Green's function G^0 for given H^0 . It is

$$G^0(\mathbf{r}, \mathbf{r}', \omega) = \sum_i \frac{\Psi_i(\mathbf{r}) \Psi_i^*(\mathbf{r}')}{\omega - \varepsilon_i \pm i\delta}, \quad (9)$$

where $\{\varepsilon_i, \Psi_i\}$ are eigenvalues and eigenfunctions of H^0 .

- (II) Calculate the dynamical screened Coulomb interaction W as

$$W = \varepsilon^{-1} v = (1 - v\Pi)^{-1} v, \quad (10)$$

where we use the proper polarization $\Pi = -iG^0 \times G^0$.

- (III) Calculate the self-energy $\Sigma(\mathbf{r}, \mathbf{r}', \omega)$ as

$$\Sigma(\mathbf{r}, \mathbf{r}', \omega) = \frac{i}{2\pi} \int d\omega' G^0(\mathbf{r}, \mathbf{r}', \omega - \omega') W(\mathbf{r}, \mathbf{r}', \omega') e^{-i\delta\omega'}. \quad (11)$$

- (IV) Simultaneously, we can calculate V^{H} for electron density from G^0 . Together with $V^{\text{ext}} + V^{\text{H}}$, we have $H(\omega) = \frac{-\nabla^2}{2m} + V^{\text{ext}} + V^{\text{H}} + \Sigma(\omega)$. The conventional one-shot GW evaluates its (usually diagonal) expectation values.

- (IV) From $\Sigma(\mathbf{r}, \mathbf{r}', \omega)$, we obtain V^{xc} through Eq. (7).

- (V) For V^{xc} , we obtain a new H^0 as $H^0 = \frac{-\nabla^2}{2m} + V^{\text{ext}} + V^{\text{H}} + V^{\text{xc}}$. From this, we do again from (I).

We repeat these steps until converged. In the procedure (I), we assume a non-interacting ground state by filling electrons up to the Fermi energy. The self-consistency ensures that this ground state is stable as for the GW approximation.

We emphasize the ability of the non-locality of the one-particle potential $V^{\text{eff}}(\mathbf{r}, \mathbf{r}')$ to describe QPs, in comparison with the ability of the local potential used in GGA/LDA. The non-locality may be classified to two kinds. One is the onsite non-locality which can be also partially described by U of LDA+ U . We have to introduce such a onsite non-local potential for the exchange-correlation term to enhance the size of orbital magnetic moment³¹, because local potential can not give the time-reversal symmetry. The other is the offsite non-locality that is important to give the difference of eigenvalues between bonding and anti-bonding orbitals. For example, we can imagine a non-local potential which behaves as a projector to push down only eigenvalues of the bonding orbital. A local potential can hardly give this effect.

The QSGW method can be justified from a view of the $G\Gamma$ theory which takes into account the vertex Γ ; Ishii, Maebashi and Takada³² gave analyses for the effects of the vertex Γ in the self-energy and in the polarization function. They claim that the effect of Γ is virtually cancelled out. An illustration of their claim is for the renormalization factor Z contained in G ; in the calculation of $\Sigma = G \times W \times \Gamma$, this Z contained in G is cancelled out by the vertex Γ , which is reduced to be $1/Z$ at $\mathbf{q}, \omega \rightarrow 0$. That is, we see the cancellation $Z \times 1/Z$ for the QP weights in $G \times \Gamma$ ²². This illustration is generalized by the Ward identity, and they concluded that we should use $\Sigma = G_0 \times W$ rather than $\Sigma = G \times W$ when we neglect vertex correction ($\Gamma = 1$). Along the context of QSGW, we interpret their theory as "If we have a good H^0 which nearly describes the QPs, we can calculate good self-energy to determine the QPs by $\Sigma = G_0 \times W$ ". Although they gave no discussion about how to obtain H^0 , we think that QSGW is a possible candidate to determine such a H^0 . As for the polarization function, they also give a discussion not to use $\Pi = -iG \times G$ but to use $\Pi = -iG_0 \times G_0$ for the proper polarization. This is reasonable because $\Pi = -iG \times G$ contains the QP electron-hole excitations with too small weight $Z_{\text{occupied}} \times Z_{\text{unoccupied}}$. This discussion for the proper polarization is consistent with the fact that first-principles calculations of dielectric functions with $\Pi = -iG_0 \times G_0$ gives good agreements with experiments³³ (and the agreements are improved by taking into account the two-body correlations in the Bethe-Salpeter equation). On the other hand, numerical calculations by Bechstedt et al³⁴ showed that poorness of $\Pi = -iG \times G$ is corrected if we include the contribution of Γ to Π . This is consistent with our claim here. The

discussions here gives a support of QSGW rather than the full self-consistent *GW* methods¹⁻⁵.

Let us consider two effects which are missing in the QSGW method. One is the effect not in the *GW* method utilized in the method (i) (or, almost equivalently, how to improve $W(\omega)$ in the step (II)). QSGW, for example, tends to give a slightly larger band gap than experimental one²², which is traced back to slightly strong $W(\omega)$ (slightly small screening effect) in the RPA. Thus, we need better $W(\omega)$ beyond the RPA. Along this line, some works are performed until now: $W(\omega)$ including pair excitations¹⁶; $W(\omega)$ including phonons³⁵; $W(\omega)$ including a vertex correction³². The other missing effects are, e.g., the contribution to the self-energy due to the low energy excitations such as the magnetic fluctuations and phonons. Note that QSGW gives QPs, where charge fluctuation is already taken into account in the RPA self-consistently. Thus we expect that the main missing contribution comes from the low energy excitations. If such contribution to the self-energy is taken into account, the QP dispersion near the Fermi energy can be deformed; kink-like structure (mass enhancement) is added just

near the Fermi energy³⁶ on top of the QP dispersion of QSGW as long as the effects due to such fluctuations is not too large. From the opposite point of view, this means that QSGW describes overall feature of energy bands including the Fermi surface except such mass enhancement near the Fermi energy. Such low energy part of self-energy may be calculated with $W(\omega = 0)$ (neglecting energy dependence) based on the many-body perturbation theory, although we need to avoid double counting problem of the Feynman diagrams intrinsic in the first-principles many-body perturbation theory³⁷. Not so much research have been performed along this line, in contrast to the first-principles method combined with the dynamical mean field theory³⁸.

Let us discuss about the total energy in QSGW. Formally, the total energy can be given by an adiabatic connection, usually specified by a parameter λ changing from zero through unity as $\hat{H}^\lambda = \hat{H}^0 + (\lambda\hat{V}^{ee} - \hat{V}_\lambda^{\text{eff}})$; this path starts from \hat{H}^0 at $\lambda = 0$, and ends with \hat{H} at $\lambda = 1$ (note that \hat{H}^0 and $\hat{V}_{\lambda=1}^{\text{eff}}$ are the second-quantized expressions of H^0 and V^{eff}). Along the path, $\hat{V}_\lambda^{\text{eff}}$ is supposed to be chosen so that QSGW applied to \hat{H}^λ gives \hat{H}^0 for any λ . Then the total energy is given as

$$E = E^0 + \int_0^1 d\lambda \frac{dE^\lambda}{d\lambda} = E^0 + \int_0^1 d\lambda \langle 0_\lambda | \hat{V}^{ee} | 0_\lambda \rangle - \int_0^1 d\lambda \langle 0_\lambda | \frac{\partial \hat{V}_\lambda^{\text{eff}}}{\partial \lambda} | 0_\lambda \rangle, \quad (12)$$

where $|0_\lambda\rangle$ is the ground state for \hat{H}^λ . Eq.(12) is an exact formula without approximation. As the lowest order approximation, we replace $|0_\lambda\rangle$ with $|0_{\lambda=0}\rangle$. Then we have the Hartree-Fock energy calculated from the eigenfunctions of H^0 . As a more accurate approximation, we evaluate $\langle 0_\lambda | \hat{V}^{ee} | 0_\lambda \rangle$ in the random phase approximation (RPA); we apply it to \hat{H}^0 whose ground state is $|0\rangle$, with the interaction of $\lambda\hat{V}^{ee}$. This gives the polarization function $\Pi(1 - \lambda v\Pi)^{-1}$, where $\Pi(\omega)$ is the polarization function of the non-interacting ground state $|0\rangle$. Then we have the RPA total energy,

$$E^{\text{RPA}} = E_0^{\text{k}} + E_0^{\text{ext}} + E_0^{\text{H}} + E_0^{\text{x}} + E^{\text{c}}, \quad (13)$$

$$E^{\text{c}} = \frac{-i}{2} \text{Tr}[\log(1 - v\Pi) + v\Pi]. \quad (14)$$

The derivative of E^{RPA} with respect to the number of occupation for the orbital $\{\epsilon_i, \Psi_i\}$ gives

$$\frac{\partial E^{\text{RPA}}}{\partial n_i} = \langle \Psi_i | \Sigma(\epsilon_i) | \Psi_i \rangle - \frac{\nabla^2}{2m} + V^{\text{ext}} + V^{\text{H}} + \Sigma(\epsilon_i) | \Psi_i \rangle. \quad (15)$$

Since $\langle \Psi_i | \Sigma(\epsilon_i) | \Psi_i \rangle$ are the diagonal elements of Eq. (7), this change (derivative) of the RPA energy equals to the QP energy given by the QSGW. In addition, the minimization of right-hand side of Eq. (15) as a functional of Ψ_i gives Eq. (5) if we can neglect Ψ_i contained in $\Sigma(\epsilon_i)$. These show that the QSGW is related to the 'RPA' total

energy. We need caution to the meaning of the QP energy ϵ_i . It is not the change of the total energy for one electron added/removed, but the derivative for occupancy. This is common to the case of the Koopman-Slater-Janak's theorem. This is related to the localization-delocalization problem³⁹, where we need to know how the eigenvalue ϵ_i changes as a function of fractional occupancy. One must recognize that ϵ_i must be calculated for the fractional occupancy, where we expect that ϵ_i changes relatively linearly, and be integrated with changing the occupancy^{18,19} in order to calculate ionization energies and so on.

Originally the QSGW is proposed to treat solids, however, we today have requirement to treat molecules on surface for such problems like catalysis. In the case of molecules (zero-dimensional systems), there are not only continuous eigenvalues but also discrete ones in H^0 . Even in this case, Eq. (5) is the equation to determine eigenstates of the system. However, it is not trivial whether we can extract the independent-particle (or the QP) picture in the manner of QSGW. Only limited number of publications on the QSGW applying to molecules are available now^{18,19}, and not so much have been clarified yet.

III. IMPLEMENTATION

In Sec. III A, we show overview of the method to perform the *GW* calculation. We made some improvements to the method in Refs.8 and 22, where we take some ideas from another *GW* implementation given by Friedrich, Blügel, and Schindlmayr⁴⁰.

In Sec. III B, we show new improvement to the offset- Γ method, which is in order to treat $\mathbf{k} \rightarrow 0$ divergence of integrand for the self-energy calculation. This improvement can correctly capture anisotropy of the screened Coulomb interaction, although the previous offset- Γ method in FP-LMTO-QSGW²² is dangerous to treat anisotropic systems.

In Sec. III C, we explain the interpolation of $V_{\mathbf{k}}^{xc}(\mathbf{r}, \mathbf{r}')$. The interpolation procedure is simplified in comparison with that used in FP-LMTO-QSGW.

A. overview

In the PMT method²⁹, the valence eigenfunctions for given H^0 are represented in the linear combinations of the Bloch summed MTOs $\chi_{\mathbf{R}Lj}^{\mathbf{k}}(\mathbf{r})$ and the APWs $\chi_{\mathbf{G}}^{\mathbf{k}}(\mathbf{r})$;

$$\Psi_{\mathbf{k}n}(\mathbf{r}) = \sum_{\mathbf{R}Lj} z_{\mathbf{R}Lj}^{\mathbf{k}n} \chi_{\mathbf{R}Lj}^{\mathbf{k}}(\mathbf{r}) + \sum_{\mathbf{G}} z_{\mathbf{G}}^{\mathbf{k}n} \chi_{\mathbf{G}}^{\mathbf{k}}(\mathbf{r}), \quad (16)$$

where we use indexes of wave vector \mathbf{k} , band index n , reciprocal lattice vector \mathbf{G} . The MTOs in the primitive cell are specified by index of MT site \mathbf{R} , angular momentum $L = (l, m)$, and j for radial functions. As for core eigenfunctions, we calculate them in the condition that they are restricted within MTs. Then we consider contributions of the cores only to the exchange part defined in Eq. (23) in the followings. (In other words, we apply core1 treatment in Ref.22 for all cores.)

In Ref.29, we have tested variety of basis sets of MTOs with APWs, whose numbers are specified by the APW cutoff energy $E_{\text{MAX}}^{\text{APW}}$. Then we show a simple and systematic procedure to choose the MTO basis sets in Ref.30. With the procedure, we can perform stable and accurate calculations. In the procedure, we use a large set of MTOs (two or three MTOs per L for valence electrons) together with APWs with rather low cutoff energy, typically, ~ 4 Ry. Thanks to the APWs, we can include only highly localized MTOs. For the damping factors $\propto \exp(-\kappa r)$ contained in MTOs, we use $\kappa^2 = 1.0$ and 2.0 (bohr)⁻². In Ref.30, we have shown that it is not necessary to optimize the κ parameters when we use large enough $E_{\text{MAX}}^{\text{APW}}$ (~ 4 Ry) as shown in Fig.1 of Ref.30. Other parameters to specify MTOs are also fixed in a simple manner. The smoothing radii of the smooth Hankel functions, which are the envelope function of the MTOs, are set to be one half of the MT radii. Thus the MTOs are chosen essentially automatically, and the convergence is checked only by $E_{\text{MAX}}^{\text{APW}}$. In addition, we do not need to use ESs because APWs is substituted for the

MTO basis of ESs. We have shown that such basis set works well in practice to determine the atomization energies of homonuclear dimers from H₂ through Kr₂ with the convergence of chemical accuracy ~ 1 Kcal/mol or less in the DF calculation in the PBE exchange correlation functional in a large supercell²⁹. Note that such supercell calculations are tough tests for augmented wave methods (FP-LAPW requires very high $E_{\text{MAX}}^{\text{APW}}$ because of small MT radius; it is not easy to apply FP-LMTO because of no way to fill ESs). In comparison with methods only using the localized basis set such as **Gaussian** in quantum chemistry, the PMT method is advantageous in the point that it can describe scattering states (higher than zero level) accurately.

At first, we re-expand $\Psi_{\mathbf{k}n}(\mathbf{r})$ in Eq. (16) as a sum of the augmentation parts in the MTs and the PW parts in the interstitial region.

$$\Psi_{\mathbf{k}n}(\mathbf{r}) = \sum_{\mathbf{R}u} \alpha_{\mathbf{R}u}^{\mathbf{k}n} \varphi_{\mathbf{R}u}^{\mathbf{k}}(\mathbf{r}) + \sum_{\mathbf{G}} \beta_{\mathbf{G}}^{\mathbf{k}n} P_{\mathbf{G}}^{\mathbf{k}}(\mathbf{r}), \quad (17)$$

where the interstitial plane wave (IPW) is defined as

$$P_{\mathbf{G}}^{\mathbf{k}}(\mathbf{r}) = \begin{cases} 0 & \text{if } \mathbf{r} \in \text{any MT} \\ \exp(i(\mathbf{k} + \mathbf{G}) \cdot \mathbf{r}) & \text{otherwise} \end{cases} \quad (18)$$

and $\varphi_{\mathbf{R}u}^{\mathbf{k}}(\mathbf{r})$ are Bloch sums of the atomic functions $\varphi_{\mathbf{R}u}(\mathbf{r})$ defined within the MT at R ,

$$\varphi_{\mathbf{R}u}^{\mathbf{k}}(\mathbf{r}) \equiv \sum_{\mathbf{T}} \varphi_{\mathbf{R}u}(\mathbf{r} - \mathbf{R} - \mathbf{T}) \exp(i\mathbf{k} \cdot \mathbf{T}). \quad (19)$$

\mathbf{T} and \mathbf{G} are lattice translation vectors in real and reciprocal space, respectively.

In the *GW* calculation, we need not only the basis set for eigenfunctions, but also the basis set to expand the product of eigenfunctions. The basis is called as the mixed product basis (MPB) $\{M_I^{\mathbf{k}}(\mathbf{r})\}$ first introduced in Ref.8. The MPB consists of the product basis (PB) within MTs¹⁰ and the IPW in the interstitial region. Since $\{M_I^{\mathbf{k}}(\mathbf{r})\}$ contains IPWs which are not orthogonal, we define dual for $\{M_I^{\mathbf{k}}(\mathbf{r})\}$ as

$$|\tilde{M}_I^{\mathbf{k}}\rangle \equiv \sum_{I'} |M_{I'}^{\mathbf{k}}\rangle (O^{\mathbf{k}})^{-1}_{I'I}, \quad (20)$$

$$O_{I'I}^{\mathbf{k}} = \langle M_{I'}^{\mathbf{k}} | M_I^{\mathbf{k}} \rangle. \quad (21)$$

From $v_{IJ}^{\mathbf{k}} = \langle M_I^{\mathbf{k}} | v | M_J^{\mathbf{k}} \rangle$, we calculate eigenfunction for the generalized eigenvalue problem defined by $\sum_J (v_{IJ}^{\mathbf{k}} - v_{\mu}^{\mathbf{k}} O_{IJ}^{\mathbf{k}}) w_{\mu J}^{\mathbf{k}} = 0$ where $v_{\mu}^{\mathbf{k}}$ are the eigenvalues of the Coulomb interaction matrix. Then we have the Coulomb interaction represented by matrix elements as

$$v(\mathbf{k}) = \sum_{\mu} |E_{\mu}^{\mathbf{k}}\rangle v_{\mu}(\mathbf{k}) \langle E_{\mu}^{\mathbf{k}}|, \quad (22)$$

where we define a new MPB $|E_{\mu}^{\mathbf{k}}(\mathbf{r})\rangle = \sum_J |M_J^{\mathbf{k}}\rangle w_{\mu J}^{\mathbf{k}}$ which is orthonormal and is diagonal to the Coulomb interaction $v(\mathbf{k})$. For the all-electron full-potential *GW* approximation, Eq. (22) is introduced in Ref.40. This

corresponds to the representation in the plane wave expansion $v(\mathbf{k} + \mathbf{G}, \mathbf{k} + \mathbf{G}') = \frac{4\pi\delta_{\mathbf{G}\mathbf{G}'}}{|\mathbf{k} + \mathbf{G}|^2}$. $\mu = 1$ corresponds

to the largest eigenvalue of v_μ , and $v_{\mu=1}$ is $\sim \frac{4\pi e^2}{|\mathbf{k}|^2}$, which is related to the divergent term discussed in Sec.III B.

With the definition of $\langle A|B\rangle = \int d^3r A^*(\mathbf{r})B(\mathbf{r})$, the exchange part of $\Sigma(\omega)$ is written as

$$\Sigma_{nm}^x(\mathbf{q}) = \langle \Psi_{\mathbf{q}n} | \Sigma_x | \Psi_{\mathbf{q}m} \rangle = - \sum_{\mathbf{k}} \sum_{n'}^{\text{BZ occ}} \langle \Psi_{\mathbf{q}n} | \Psi_{\mathbf{q}-\mathbf{k}n'} E_\mu^{\mathbf{k}} \rangle v_\mu(\mathbf{k}) \langle E_\mu^{\mathbf{k}} \Psi_{\mathbf{q}-\mathbf{k}n'} | \Psi_{\mathbf{q}m} \rangle. \quad (23)$$

The screened Coulomb interaction $W(\omega)$ is calculated through Eq. (10), where the polarization function $\Pi(\omega)$ is written as

$$\begin{aligned} \Pi_{\mu\nu}(\mathbf{q}, \omega) = & \sum_{\mathbf{k}}^{\text{BZ}} \sum_n^{\text{occ}} \sum_{n'}^{\text{unocc}} \frac{\langle E_\mu^{\mathbf{q}} \Psi_{\mathbf{k}n} | \Psi_{\mathbf{q}+\mathbf{k}n'} \rangle \langle \Psi_{\mathbf{q}+\mathbf{k}n'} | \Psi_{\mathbf{k}n} E_\nu^{\mathbf{q}} \rangle}{\omega - (\varepsilon_{\mathbf{q}+\mathbf{k}n'} - \varepsilon_{\mathbf{k}n}) + i\delta} \\ & + \sum_{\mathbf{k}}^{\text{BZ}} \sum_n^{\text{unocc}} \sum_{n'}^{\text{occ}} \frac{\langle E_\mu^{\mathbf{q}} \Psi_{\mathbf{k}n} | \Psi_{\mathbf{q}+\mathbf{k}n'} \rangle \langle \Psi_{\mathbf{q}+\mathbf{k}n'} | \Psi_{\mathbf{k}n} E_\nu^{\mathbf{q}} \rangle}{-\omega - (\varepsilon_{\mathbf{k}n} - \varepsilon_{\mathbf{q}+\mathbf{k}n'}) + i\delta}. \end{aligned} \quad (24)$$

When time-reversal symmetry is assumed, $\Pi(\omega)$ can be simplified to read

$$\begin{aligned} \Pi_{\mu\nu}(\mathbf{q}, \omega) = & \sum_{\mathbf{k}}^{\text{BZ}} \sum_n^{\text{occ}} \sum_{n'}^{\text{unocc}} \langle E_\mu^{\mathbf{q}} \Psi_{\mathbf{k}n} | \Psi_{\mathbf{q}+\mathbf{k}n'} \rangle \langle \Psi_{\mathbf{q}+\mathbf{k}n'} | \Psi_{\mathbf{k}n} E_\nu^{\mathbf{q}} \rangle \\ & \times \left(\frac{1}{\omega - \varepsilon_{\mathbf{q}+\mathbf{k}n'} + \varepsilon_{\mathbf{k}n} + i\delta} - \frac{1}{\omega + \varepsilon_{\mathbf{q}+\mathbf{k}n'} - \varepsilon_{\mathbf{k}n} - i\delta} \right). \end{aligned} \quad (25)$$

To evaluate Eq. (24) or Eq. (25), we first accumulate its imaginary parts (anti-Hermitian part) of $\Pi_{\mu\nu}(\mathbf{q}, \omega)$ along bins of histograms on the real axis ω with the tetrahedron technique⁴¹, and then determines the real part via the Hilbert transformation. The bins are dense near the Fermi energy and coarse at high energy as described in Ref.22. This procedure is not only more efficient but also safer than methods to calculate the real part directly. We also use the extended irreducible zone (EIBZ) symmetrization procedure described in Ref.40.

The correlation part of the screened Coulomb interaction $W^c(\omega) = W(\omega) - v$, which is calculated from v and $\Pi(\omega)$ is given as

$$W^c(\mathbf{k}, \omega) = \sum_{\mu\nu} |E_\mu^{\mathbf{k}} \rangle W_{\mu\nu}^c(\mathbf{k}, \omega) \langle E_\mu^{\mathbf{k}}|. \quad (26)$$

With this $W^c(\mathbf{k}, \omega)$, we have the correlation part of the self-energy as

$$\Sigma_{n,n'}^c(\mathbf{q}, \omega) = \sum_{\mathbf{k}, m} \int_{-\infty}^{\infty} d\omega' \sum_{\mu, \nu} \frac{\langle \Psi_{\mathbf{q}n} | \Psi_{\mathbf{q}-\mathbf{k}m} E_\mu^{\mathbf{k}} \rangle W_{\mu\nu}^c(\mathbf{k}, \omega') \langle E_\nu^{\mathbf{k}} \Psi_{\mathbf{q}-\mathbf{k}m} | \Psi_{\mathbf{q}n'} \rangle e^{-i\delta\omega'}}{\omega - \omega' - \varepsilon_{\mathbf{q}-\mathbf{k}m} \pm i\delta}. \quad (27)$$

Here, we use $+i\delta$ for occupied states of $\mathbf{q}-\mathbf{k}m$, $-i\delta$ for unoccupied states. In QSGW, we have to calculate Hermitian part of $\Sigma_{nn'}^c(\mathbf{q}, \varepsilon_{\mathbf{q}n})$, in order to obtain $V_{\mathbf{q}}^{\text{xc}}$ via Eq. (7).

There are two key points to handle the GW procedure given above. The first key point, given in Sec.III B, is the improved offset- Γ method which treats divergence of $W^c(\mathbf{k} \rightarrow 0, \omega)$ in Eq. (27). For this purpose, we define non-divergent effective interaction $\overline{W}^c(\mathbf{k} = 0, \omega)$ instead of $W^c(\mathbf{k} = 0, \omega)$. Then we can take simple discrete sum for both expressions of Eq. (23) and Eq. (27).

The second point in Sec.III C is how to make an interpolation to give $V_{\mathbf{q}}^{\text{xc}}$ at any \mathbf{q} in the whole BZ, from $V_{\mathbf{q}}^{\text{xc}}$ calculated only at limited numbers of \mathbf{q} points. This is required in the offset- Γ method shown in Sec.III B, that

is, we have to calculate eigenfunctions at some \mathbf{q} points near $\mathbf{q} = 0$. For the interpolation, we expand the static non-local potential V^{xc} in Eq. (7) in the highly-localized MTOs in the real space. Thus the MTOs are used for two purposes; one is as the bases for the eigenfunctions, the other is as the bases to expand V^{xc} . The interpolation procedure of $V_{\mathbf{k}}^{\text{xc}}(\mathbf{r}, \mathbf{r}')$ becomes stabilized and simplified rather than the complicated interpolation procedure in Ref.22. This is because we now use highly localized MTOs. In the planewave-based QSGW method by Hamann and Vanderbilt¹⁵, they expand V^{xc} in the maximally localized Wannier functions instead of the MTOs.

In practical implementation, the LDA or GGA exchange-correlation potential $V_{\text{LDA}}^{\text{xc}}$ is used as an assistance in order to generate core eigenfunctions and

also the radial functions within the MTs (in this paper, we use subscript LDA even in the GGA. ‐LDA/GGA‐ means LDA or GGA). The difference $V^{\text{xc}} - V_{\text{LDA}}^{\text{xc}}$ is used for the interpolation procedure in the BZ (explained in Sec.III C), because this difference is numerically small as long as $V_{\text{LDA}}^{\text{xc}}$ is not so bad approximation. These procedures with $V_{\text{LDA}}^{\text{xc}}$ give a slight dependence to the final numerical results in practice as seen in Sec.IV, although the results formally does not depend on the LDA/GGA exchange-correlation functions anymore.

B. Improve offset- Γ method

The offset- Γ method, originally invented for Ref.8 by Kotani (described in Ref.22), was a key to perform accurate GW calculation. It is for integration of \mathbf{k} in Eq. (23) and Eq.(27), where we have the integrands diverge at $\mathbf{k} \rightarrow 0$. It worked well for highly symmetric systems, however, it can be problematic to apply less symmetric systems, because anisotropic divergence of the integrands may not be treated accurately. Here we show an improved offset- Γ method, which treat anisotropy of $W(\mathbf{k}, \omega)$ accurately. In the followings, we use expression $W(\mathbf{k})$ for simplicity (omit subscripts and ω) instead of $W_{\mu\nu}(\mathbf{k}, \omega)$, since we concern the \mathbf{k} integral.

Let us give a formula to calculate $\int_{\text{BZ}} f(\mathbf{k}) d^3k$ by discrete sum on \mathbf{k} -mesh, where $f(\mathbf{k}) = G(\mathbf{q} - \mathbf{k}) \times W(\mathbf{k})$. As the \mathbf{k} -mesh, we use

$$\mathbf{k}(i_1, i_2, i_3) = 2\pi \left(\frac{i_1}{N_1} \mathbf{b}_1 + \frac{i_2}{N_2} \mathbf{b}_2 + \frac{i_3}{N_3} \mathbf{b}_3 \right),$$

where $\mathbf{b}_1, \mathbf{b}_2$ and \mathbf{b}_3 are the primitive reciprocal vectors (the same as the Eq.(47) in Ref.22). The 1st BZ is divided into $N = N_1 \times N_2 \times N_3$ microcells ($i_1 = 0, 1, \dots, N_1 - 1$. Also the same for i_2 , and i_3). The microcell including the Γ point is called as the Γ cell⁴². Main problem is how to evaluate the contribution from the Γ cell. The divergent part of $f(\mathbf{k})$ behaves \approx (analytic function of \mathbf{k}) / $(\mathbf{k}^T \mathbf{L} \mathbf{k})$, where \mathbf{k}^T means the transpose of \mathbf{k} , \mathbf{L} is an 3×3 Hermitian matrix⁴⁰. We neglect an odd part of \mathbf{k} in the above (analytic function of \mathbf{k}) because it gives no contribution to the integral around $\mathbf{k} = 0$. Thus it is enough to consider integral for $f(\mathbf{k})$ whose divergent parts behaves $f(\mathbf{k}) = \sum_L \frac{f_L Y_L(\hat{\mathbf{k}})}{|\mathbf{k}|^2}$ at $\mathbf{k} \rightarrow 0$, where l of $L \equiv (l, m)$ are restricted to be even number. We evaluate the integral by a formula

$$\int_{\text{BZ}} f(\mathbf{k}) d^3k \approx \frac{1}{N} \sum_{\mathbf{k} \neq 0} f(\mathbf{k}) + \sum_L f_L w_L + \frac{1}{N} \tilde{f}, \quad (28)$$

which is introduced in Ref.42. Here weights w_L are determined in a manner as follows, so as to take into account contributions of divergent part of $f(\mathbf{k})$ at $\mathbf{k} \rightarrow 0$ in the Γ cell. \tilde{f} is the constant part of $f(\mathbf{k})$ at $\mathbf{k} \rightarrow 0$.

To determine w_L , we can use the following procedure instead of that given in Ref.42. We first introduce auxil-

iary functions

$$F_L(\mathbf{k}) = \sum_{\mathbf{G}} \frac{\exp(-\alpha |\mathbf{k} - \mathbf{G}|^2) Y_L(\widehat{\mathbf{k} - \mathbf{G}})}{|\mathbf{k} - \mathbf{G}|^2}. \quad (29)$$

This is a generalization of an auxiliary function used in the offset- Γ method (then we only used F_{00} ²²). We usually take $\alpha \rightarrow 0$ limit, or small enough α instead. Let us apply Eq. (28) to $F_L(\mathbf{k})$. Then we can evaluate the left hand side of Eq. (28) exactly (the exact values are zero except $L = (0, 0)$). On the other hand, the first term and the third term in the right-hand side of Eq. (28) can be evaluated numerically. In addition, we know that $f_{L'}$ for $F_L(\mathbf{k})$ is unity for $L' = L$, and zero otherwise. Thus we can determine w_L in Eq. (28) so that Eq. (28) is exactly satisfied for $F_L(\mathbf{k})$ for any L .

Let us apply Eq. (28) to $f(\mathbf{k}) = G(\mathbf{q} - \mathbf{k}) \times W(\mathbf{k})$. Then we make an approximation taking only the most divergent term in $W(\mathbf{k})$ in addition to its analytic part. That is, we use

$$W_{\mu\nu}(\mathbf{k}) \sim \widetilde{W}_{\mu\nu}(\mathbf{0}) + \frac{4\pi}{\mathbf{k}^T \mathbf{L} \mathbf{k}} \delta_{1\mu} \delta_{1\nu} \quad (30)$$

at $\mathbf{k} \rightarrow 0$. $\widetilde{W}_{\mu\nu}(\mathbf{0}) = 0$ for $\mu = 1$ or $\nu = 1$. See Eq.(36) in Ref.40 to know what is neglected in the approximation of Eq. (30).

Then we finally obtain

$$\int_{\text{BZ}} d^3k G(\mathbf{q} - \mathbf{k}) W(\mathbf{k}) \approx \overline{\sum G(\mathbf{q} - \mathbf{k}) W(\mathbf{k})}, \quad (31)$$

where its right-hand side is defined as

$$\begin{aligned} & \overline{\sum G(\mathbf{q} - \mathbf{k}) W(\mathbf{k})} \\ & \equiv \frac{1}{N} \sum_{\mathbf{k} \neq 0} G(\mathbf{q} - \mathbf{k}) W(\mathbf{k}) + \frac{1}{N} G(\mathbf{q}) \overline{W}(\mathbf{0}), \end{aligned} \quad (32)$$

$$\overline{W}(\mathbf{0}) \equiv N \sum w_L W_L + \widetilde{W}(\mathbf{0}). \quad (33)$$

Here $\overline{W}(\mathbf{0})$ can be taken as an averaged W in the Γ cell. With this $\overline{W}(\mathbf{0})$, we can evaluate integrals just by sum on discrete \mathbf{k} -mesh. When the matrix \mathbf{L} is given (a method to calculate \mathbf{L} is given in the next paragraph), the non-analytic (but non-divergent) function $\mathbf{k}^T \mathbf{L} \mathbf{k} / |\mathbf{k}|^2$ is expanded in the spherical harmonics. Then W_L is calculated for the given \mathbf{L} in the manner of Ref.40. We can evaluate the accuracy of integrals with discrete \mathbf{k} -mesh in combination with the approximation Eq. (30) by calculations with changing the size of the \mathbf{k} -mesh.

The remaining problem is how to calculate the matrix \mathbf{L} in Eq. (30). There are two possible ways to determine it. One is the $\mathbf{k} \cdot \mathbf{p}$ method (perturbation) used in⁴⁰, the other is numerical method to determine them by calculations at some \mathbf{k} points near $\mathbf{k} = 0$. Here we use the latter method. Because of the point-group symmetry of the system, \mathbf{L} can be expressed by the linear combination of invariant tensors μ_{ij}^g for the symmetry of the unit cell;

$$L_{ij}(\omega) = \sum_{g=1}^{N_g} a_g(\omega) \mu_{ij}^g, \quad (34)$$

where g is the index of invariant tensor. The number of g , N_g , can be from one (cubic symmetry) through six (no symmetry). It is possible to determine coefficient $a_g(\omega)$ from the dielectric functions $\hat{\mathbf{k}}_{0i}^T \mathbf{L} \hat{\mathbf{k}}_{0i}$ calculated at $\{\mathbf{k}_{0i}\}$ points around $\mathbf{k} = 0$, where $\{\mathbf{k}_{0i}; i = 1, N_g\}$ is a set of the offset- Γ points. The offset- Γ points are chosen so that conversion matrix from $\hat{\mathbf{k}}_{0i}^T \mathbf{L}(\omega) \hat{\mathbf{k}}_{0i}$ to $a_g(\omega)$ should not numerically degenerated. The length $|\mathbf{k}^{0i}|$ can be chosen to be small enough, but avoiding numerical error as the average of $W(\mathbf{k})$ in the Γ cell. The improved offset- Γ method shown here can be applicable even to metal cases, as long as $\hat{\mathbf{k}}_{0i}^T \mathbf{L}(\omega) \hat{\mathbf{k}}_{0i}$ contains the contribution due to intraband transition.

C. Interpolation of the self-energy in the Brillouin zone

Here we show an interpolation procedure to give $V_{\mathbf{k}}^{\text{xc}}$ at any \mathbf{k} , from $V_{\mathbf{k}}^{\text{xc}}$ calculated only at the regular mesh points $\mathbf{k}(i_1, i_2, i_3)$. This interpolation is used for the offset- Γ method that requires $W(\omega)$ at $\{\mathbf{k}_{0i}\}$; to calculate these $W(\omega)$, we need eigenfunctions and eigenvalues not only at the regular mesh points $\mathbf{k}(i_1, i_2, i_3)$, but also at $\mathbf{k}(i_1, i_2, i_3) + \mathbf{k}_{0i}$. This interpolation is also useful to plot energy bands, thus to obtain effective mass and so on. A key point of the interpolation is that V^{xc} is expanded in real space in the highly localized MTOs as follows.

At the end of the step of (IV) in Sec.II, we obtain the matrix elements $\langle \Psi_{\mathbf{k}n} | \Delta V_{\mathbf{k}}^{\text{xc}} | \Psi_{\mathbf{k}m} \rangle$ on the regular mesh points of \mathbf{k} , where $\Delta V_{\mathbf{k}}^{\text{xc}} = V_{\mathbf{k}}^{\text{xc}} - V_{\mathbf{k}}^{\text{xc,LDA}}$. Then it is converted to the representation in the APW and MTO bases as

$$\langle \chi_a^{\mathbf{k}} | \Delta V_{\mathbf{k}}^{\text{xc}} | \chi_b^{\mathbf{k}} \rangle = \sum_{n,m} (z^{-1})_{an}^* \langle \Psi_{\mathbf{k}n} | \Delta V_{\mathbf{k}}^{\text{xc}} | \Psi_{\mathbf{k}m} \rangle z_{bm}^{-1}, \quad (35)$$

where we use simplified basis index a , which is the index to specify a basis ($\mathbf{R}Lj$ for MTO or \mathbf{G} for APW). Thus $\chi_a^{\mathbf{k}}$ denotes the APWs or MTOs in Eq. (16); $z_{na}(\mathbf{k})$ (is omitted for simplicity) means the coefficients of the eigenfunctions at \mathbf{k} , that is, $z_{\mathbf{R}Lj}^{\mathbf{k}n}$ and $z_{\mathbf{G}}^{\mathbf{k}n}$ in Eq. (16) together. This z_{an} is identified as a conversion matrix which connect eigenfunctions (band index n) and the APW and MTO bases (basis index a).

To obtain real space representation, we need a representation expanded in the basis that consist of the Bloch summed localized orbitals, which are periodic for \mathbf{k} in the BZ. However, this is not the case for the APWs in Eq. (35). To overcome this problem, we make an approximation that we only take the matrix elements related to the MTOs, that is, the elements $\langle \chi_a^{\mathbf{k}} | \Delta V_{\mathbf{k}}^{\text{xc}} | \chi_b^{\mathbf{k}} \rangle$ where a and b specify MTOs. The part related to APWs are not thrown away but projected onto the basis of MTOs. This approximation can be reasonable as long as main part of ΔV^{xc} can be well expanded in the MTOs, although we need numerical tests to confirm accuracy as

shown in Sec.IV. Then we obtain a real-space representation of ΔV^{xc} expanded in the MTOs from the MTO part of $\langle \chi_a^{\mathbf{k}} | \Delta V_{\mathbf{k}}^{\text{xc}} | \chi_b^{\mathbf{k}} \rangle$ by the Fourier transformation. Then we can have interpolated one by the inverse Fourier transformation from it for any \mathbf{k} . Since we use highly localized MTOs, this interpolation procedure is more stable than the previous one in the FP-LMTO-QSGW²². A complicated interpolation procedure given in Sec.II-G in Ref.22 is not necessary anymore.

To reduce computational time, we calculate $\langle \Psi_{\mathbf{k}n} | \Delta V_{\mathbf{k}}^{\text{xc}} | \Psi_{\mathbf{k}m} \rangle$ only up to the states whose eigenvalues are less than E_{MAX}^{Σ} . Then the higher energy parts of matrix elements is assumed to be diagonal, where their values are given by a constant, an average of calculated diagonal elements.

IV. NUMERICAL TEST

TABLE I. Used MTOs for GaAs and SiO2c (β -cristobalite). These are specified by the principle quantum numbers and angular momentums. The MTO's envelope functions are the smooth Hankel functions, which are specified by two parameters, the damping factor κ and the smoothing radius R_{sm} . We set the parameters in the manner of Ref.29. R_{sm} is given to be one half of the MT radius R_{MT} , which is shown in the unit of bohr radius. Empty spheres (ESs) are located in the middle of the interstitial region (two ESs per primitive cell in both of GaAs and SiO2c). ESs are used only cases specified by "vwn,es" and "pbe,es" in II and IV. Unit of κ^2 is in (bohr)⁻²

		valence	R_{MT}
GaAs			
Ga	3d(lo), 4s4p4d4f($\kappa^2=1.0$), 4s4p4d($\kappa^2=2.0$)		2.19
As	3d(lo), 4s4p4d4f($\kappa^2=1.0$), 4s4p4d($\kappa^2=2.0$)		2.30
(ES)	1s2p3d($\kappa^2=1.0$), 1s2p($\kappa^2=2.0$)		2.80
SiO2c (two Si and four O in a primitive cell)			
Si	4s4p4d4f($\kappa^2=1.0$), 4s4p4d($\kappa^2=2.0$)		2.19
O	2s3p4d($\kappa^2=1.0$), 2s3p4d($\kappa^2=2.0$)		2.30
(ES)	1s2p3d4f($\kappa^2=1.0$)		2.80

Here we show results of test calculations for PMT-QSGW applied to two examples, GaAs and the cubic SiO₂ (β -cristobalite, denoted as SiO2c hereafter). The latter has large interstitial regions; it has the same structure of Si but oxygen atoms are located in the middle of Si-Si bonds. We use lattice constants 5.653 Å for GaAs, and 7.165 Å for SiO2c. We perform calculations with different settings in order to show the convergence properties of the band gaps. We use the simple and systematic procedure to determine sets of MTOs and APWs, as is explained after Eq. (16). We use the MTOs shown in Table.I. As for Ga(3d) and As(3d), we use the local orbitals⁴³.

In advance to show the band gaps calculated in QSGW, let us show those in LDA/GGA in Table.II. We can check

TABLE II. Band gap in LDA/GGA to check the convergence on the basis set. For sets of MTOs shown in Table.I, we tabulate the calculated band gaps for $E_{\text{MAX}}^{\text{APW}}$. Note “vwn,es” and “pbe,es” means with ESs. We can see band gaps converge well with small number of APWs; this is consistent with the case of atomization energies³⁰. In the GGA case with ESs, convergence behavior becomes a little unstable (not converged for 6.0 Ry for SiO2c), because of numerical instability of linear-dependency. n_{APW} means number of APWs at $\mathbf{k} = 0$. Number of MTOs without ESs are 60 for GaAs and 168 for SiO2c.

band gap (eV) in LDA/GGA					
$E_{\text{MAX}}^{\text{APW}}$ (Ry)	vwn	vwn,es	pbe	pbe,es	n_{APW}
GaAs					
0.0	0.425	0.308	0.665	0.541	0
1.0	0.322	0.295	0.558	0.528	1
2.0	0.294	0.294	0.526	0.529	15
3.0	0.294	0.294	0.528	0.532	27
4.0	0.294	0.294	0.530	0.535	51
5.0	0.294	0.294	0.530	0.536	59
6.0	0.294	0.294	0.530	0.538	65
SiO2c					
0.0	8.560	6.131	8.592	6.186	0
1.0	5.406	5.434	5.663	5.563	15
2.0	5.437	5.445	5.670	5.622	27
3.0	5.442	5.445	5.665	5.652	59
4.0	5.444	5.446	5.665	5.668	65
5.0	5.446	5.447	5.668	5.658	113
6.0	5.446	5.445	5.669	—	169

the convergence behavior by changing the APW cutoff energy $E_{\text{MAX}}^{\text{APW}}$. For the functional of LDA, we use the VWN exchange-correlation functional⁴⁴; for GGA, we employ PBE⁴⁵; ‘vwn,es’ and ‘pbe,es’ mean cases that ESs are included. The convergence behavior is satisfactory, as was in the case of total energy for homo-nuclear dimers³⁰. We see better convergence behavior as for $E_{\text{MAX}}^{\text{APW}}$ for ‘vwn,es’ and ‘pbe,es’ than ‘vwn’ and ‘pbe’, since we have larger number of basis. For example, ‘vwn,es’ for GaAs shows 0.295 eV for $E_{\text{MAX}}^{\text{APW}}=1$ Ry is essentially the same as the converged value of 0.294 eV, while ‘vwn’ requires $E_{\text{MAX}}^{\text{APW}} \gtrsim 2$ Ry to have similar convergence. For SiO2c, the convergence is a little slower because SiO2c has large interstitial region, e.g., the band gap 5.437 eV for ‘vwn’ at $E_{\text{MAX}}^{\text{APW}} \gtrsim 2$ Ry shows ~ 0.01 eV difference from converged value of 5.445 eV (we took the case of ‘vwn,es’ at $E_{\text{MAX}}^{\text{APW}}=6$ Ry). Within this small error, we can determine the band gap even without ESs. This confirms our expectation that missing part of the Hilbert space spanned by highly localized MTOs (large damping factors $\kappa^2 = 1.0$ and 2.0 (bohr)⁻²) is complemented by the APWs with such very low $E_{\text{MAX}}^{\text{APW}}$. The wave number of the cutoff corresponds to distance between nearest-neighbor atoms. We saw a little instability (we need many iterations) in the calculations when we use $E_{\text{MAX}}^{\text{APW}} \gtrsim 5$ Ry in the case of ‘pbe,es’, since GGA requires better numerical accuracy to calculate derivative of density. This is because of the overcompleteness problem of the basis set, that is,

we lose linear-independency of basis functions for large $E_{\text{MAX}}^{\text{APW}}$. We conclude that Table.II gives a satisfactory convergence behavior within this limitation.

TABLE III. The product basis (PB) within MTs are constructed from the products of atomic basis. After all the products are generated, remove linearly-dependent ones with the use of the overlap matrix of the products. See Ref.22 in detail. l_{cut} means the allowed maximum l of the PB. n_{PB} shows the total number of PB in each MT.

		products	l_{cut}	tol	n_{PB}
GaAs					
PB0	Ga	$\phi(4s, 4p, 3d, 4d) \times \phi(4s, 4p, 3d, 4d, 4f)$	4	10^{-3}	97
	As	$\phi(4s, 4p, 3d, 4d) \times \phi(4s, 4p, 3d, 4d, 4f)$	4	10^{-3}	106
PB0t	Ga	PB0	4	10^{-5}	119
	As	PB0	4	10^{-5}	126
PB0l	Ga	PB0	6	10^{-3}	119
	As	PB0	6	10^{-3}	128
PB1	Ga	$\phi(4s, 4p, 3d, 4d) \times \phi(4s, 4p, 3d, 4d, 4f)$	4	10^{-3}	115
	As	$\phi(4s, 4p, 3d, 4d) \times \phi(4s, 4p, 3d, 4d, 4f)$	4	10^{-3}	115
		$\phi(4s, 4p, 3d, 4d) \times \phi(4s, 4p, 3d, 4d, 4f)$	4	10^{-3}	115
(ES)	$\phi(1s, 2p, 3d) \times \phi(1s, 2p, 3d, 4f)$	2	10^{-3}	22	
PB1l	Ga	PB1	6	10^{-5}	175
	As	PB1	6	10^{-5}	178
SiO2c					
PB0	Si	$\phi(3s, 3p, 3d) \times \phi(3s, 3p, 3d, 4f)$	4	10^{-3}	75
	O	$\phi(2s, 2p, 3d) \times \phi(2s, 2p, 3d, 4f)$	4	10^{-3}	67
PB0s	Si	PB0	4	10^{-3}	76
	O	PB0	2	10^{-3}	31
PB1	Si	$\phi(3s, 3p, 3d) \times \phi(3s, 3p, 3d, 4f)$	4	10^{-3}	76
	O	$\phi(3s, 3p, 3d) \times \phi(3s, 3p, 3d, 4f)$	4	10^{-3}	76
		$\phi(2s, 2p, 3d) \times \phi(2s, 2p, 3d, 4f)$	2	10^{-3}	31
(ES)	$\phi(2s, 2p, 3d) \times \phi(2s, 2p, 3d, 4f)$	2	10^{-3}	22	
PB1l	Si	PB1	4	10^{-5}	76
	O	PB1	4	10^{-5}	70

Let us summarize settings (and parameters) to perform the PMT-QSGW calculations. These can be classified into followings;

- (A) IPW cutoff $|\mathbf{q} + \mathbf{G}|_{\text{MAX}}^{\Psi}$ to give allowed $P_{\mathbf{G}}^{\mathbf{q}}(\mathbf{r})$ in the expansion of eigenfunctions Eq. (17).
- (B) Settings of the mixed product basis. We have parameters to specify product basis (PB) within MTs. The IPWs belonging to the mixed product basis is given by the cutoff $|\mathbf{q} + \mathbf{G}|_{\text{MAX}}^W$. The sets of PB are shown in Table III.
- (C) Cutoff energy for self-energy. As we explained in Sec.III C, we calculate $\langle i|\Delta V^{\text{xc}}|j\rangle$ only for $\epsilon_i \leq E_{\text{MAX}}^{\Sigma}$ and $\epsilon_j \leq E_{\text{MAX}}^{\Sigma}$, where E_{MAX}^{Σ} is measured from the top of valence. See the bottom of Sec.III C.
- (D) Energy-axis parameters for GW. These are used to accumulate imaginary part of

TABLE IV. Band gap (at Γ) for GaAs and cubic SiO2c (β -cristobalite SiO₂) in the PMT-QSGW method in different cut-offs/settings. Number of used \mathbf{k} points in the 1st BZ is $4 \times 4 \times 4$ for GaAs, and $2 \times 2 \times 2$ for SiO2c. No spin-orbit coupling. The first line named as REF is treated as a standard to compare others in this table. Empty columns mean the default settings of REF. The column $|\mathbf{q} + \mathbf{G}|_{\text{Max}}^{\Psi, W}$ shows used $|\mathbf{q} + \mathbf{G}|_{\text{Max}}^{\Psi}$ and $|\mathbf{q} + \mathbf{G}|_{\text{Max}}^W$. Lines marked by “*” show best-efforts values (largest bases). Lines marked by “**” is the case used for Fig.1.

GaAs						SiO2c					
XC	$ \mathbf{q} + \mathbf{G} _{\text{Max}}^{\Psi, W}$ (1/bohr)	PB	E_{MAX}^{Σ} (Ry)	$E_{\text{MAX}}^{\text{APW}}$ (Ry)	Band gap (eV)	XC	$ \mathbf{q} + \mathbf{G} _{\text{Max}}^{\Psi, W}$ (1/bohr)	PB	E_{MAX}^{Σ} (Ry)	$E_{\text{MAX}}^{\text{APW}}$ (Ry)	Band gap (eV)
REF:						REF:					
vwn	4.0, 3.0	PB1	all	3.0	1.939	vwn	4.0, 3.0	PB1	all	3.0	11.16
	6.0, 4.0				1.939		8.0, 6.0				11.28
	3.5, 3.0				1.940		6.0, 4.0				11.27
	3.0, 2.5				1.934		3.5, 3.0				11.15
		PB0			1.956		3.0, 2.5				10.76
		PB0t			1.938			PB0			11.20
		PB0l			1.967			PB0s			11.17
		PB1l			1.946			PB1l			11.19
				2.0	1.931			PB1l		6.0	11.21
				4.0	1.950					6.0	11.18
				5.0	1.959				3.0		10.38 **
				6.0	1.969				6.0		10.78
			3.0		1.942 **				9.0		10.99
			3.0	6.0	1.980						10.49
vwn,es					1.945					4.0	10.47
vwn,es				6.0	1.982 *					6.0	10.41 *
vwn,es			3.0		1.903				3.0		10.09
vwn,es			3.0	6.0	1.940						11.31
pbe				2.0	1.973					6.0	11.33
pbe					1.981						10.57
pbe				4.0	1.992					5.0	10.54 *
pbe				5.0	2.001						
pbe				6.0	2.010						
pbe,es					1.969						
pbe,es			3.0		1.940						
pbe,es				6.0	2.002 *						

$W(\omega)$. See the explanation around Eq. (25). We use an energy mesh (bin width); the bin width is 0.005 Ry at $\omega = 0$ and quadratically coarser at larger ω (Sec.II-D in Ref.29). The bin width becomes twiced at 0.04Ry. For integration along imaginary axis, we use ten points in the imaginary axis of ω . The parameters are good enough to give reasonable results as seen in Ref.29.

- (E) $E_{\text{MAX}}^{\text{APW}}$
- (F) Use ESs or not.
- (G) LDA or GGA, which are used as an assistance of numerical calculation in PMT-QSGW. See at the bottom of Sec.III A.

Here (E),(F) and (G) are settings in common with the LDA/GGA-level calculations.

In Table IV, we show the band gaps for GaAs and SiO2c calculated by PMT-QSGW for changing setting of (A)-(G). We calculate the self-energy only at \mathbf{k} -mesh points, which are $4 \times 4 \times 4$ and $2 \times 2 \times 2$ in the 1st BZ

for GaAs and SiO2c, respectively (we use large enough \mathbf{k} -mesh for electron density, $10 \times 10 \times 10$ for GaAs, and $6 \times 6 \times 6$ for SiO2c). No spin orbit coupling is included. In the calculation of polarization function of Eq. (25), we take all occupied and unoccupied states. The top line date labeled as 'REF', which show the gaps 1.939 eV(GaAs) and 11.16 eV(SiO2c), are treated as bases for following comparisons with other cases. For the cases of 'REF', we take all bands ('all' for the column of E_{MAX}^{Σ} means taking all the matrix elements of ΔV^{xc} , that is, E_{MAX}^{Σ} is infinity). Empty spaces in the Table IV mean that we use the same settings with the case of 'REF'. For example, the next line to REF for GaAs means a case with the same settings with REF except changes of $|\mathbf{q} + \mathbf{G}|_{\text{Max}}^{\Psi} = 6.0$ and $|\mathbf{q} + \mathbf{G}|_{\text{Max}}^W = 4.0$.

We can see following points from the Table IV. Generally speaking (as we see followings), it seems not so easy to attain numerical error within ~ 0.1 eV. Thus we take ~ 0.1 eV as our target of numerical accuracy in the PMT-QSGW method. It is not so meaningful to discuss about small differences.

1. At the first section, we can see the dependence

on $|\mathbf{q} + \mathbf{G}|_{\text{Max}}^{\Psi}$ and $|\mathbf{q} + \mathbf{G}|_{\text{Max}}^W$. We see that the REF setting, $(|\mathbf{q} + \mathbf{G}|_{\text{Max}}^{\Psi}, |\mathbf{q} + \mathbf{G}|_{\text{Max}}^W) = (4.0, 3.0)$ (bohr) $^{-1}$, show convergence of ~ 0.01 eV even for the case of SiO₂c (~ 0.001 eV for GaAs) for these parameters. We have shown similar check in Ref.22.

2. In our test cases of the PB in Table III, we can estimate numerical errors caused by the choice of PB. As for PB in GaAs, 1.939 eV given by PB1 (REF) gives good agreement with 1.946 eV by PB1*l*, which is the largest PB among what we used here. For SiO₂c, we have little dependence on the choice of the PB used here. Especially, in case of PB0s, we use a set of PB on oxygen only with $l_{\text{cut}} = 2$. This choice reduces the computational time so much for larger systems.

3. The band gap gradually increases when we increase $E_{\text{MAX}}^{\text{APW}}$ in GaAs. The band gap monotonically changes from 1.939 eV at $E_{\text{MAX}}^{\text{APW}}=3.0$ Ry to 1.969 eV at $E_{\text{MAX}}^{\text{APW}}=6.0$ Ry for 'vwn' (we see similar changes for 'vwn,es' where 1.945 eV to 1.982 eV). Thus we can not see convergence behavior within this range of $E_{\text{MAX}}^{\text{APW}}$. This 1.969 eV can be taken as the best value for 'vwn' among performed calculations in the sense of largest number of APWs. Because of over-completeness problem of basis sets in the PMT method, it is not easy to enlarge number of APWs. In addition, eigenfunctions at high energy are not accurate enough (we do not include local orbital for high energy bands). Thus we inevitably takes this behavior as a limitation of our current implementation of the PMT-QSGW. Recall that such slow convergence on the number of unoccupied bands (= number of APWs in our case) is also observed in Ref.46.

We observe similar behavior in the case of SiO₂c. The band gap of SiO₂c changes from 11.16 eV at $E_{\text{MAX}}^{\text{APW}}=3\text{Ry}$ (REF), to 11.18 eV at $E_{\text{MAX}}^{\text{APW}}=6.0$ Ry. We see similar change for 'vwn,es'; it is from 10.49 eV at $E_{\text{MAX}}^{\text{APW}}=3.0$ Ry to 10.41 eV at $E_{\text{MAX}}^{\text{APW}}=6.0$ Ry.

4. Let us discuss other points for GaAs.

At first, we see that using $E_{\text{MAX}}^{\Sigma}=3.0$ Ry (marked by **) gives little difference from REF (1.942-1.939 eV). Thus we may use $E_{\text{MAX}}^{\Sigma}=3.0$ Ry to reduce computational efforts.

We should take "vwn,es" gives better values than "vwn" because we include the MTOs of ESs as bases. We see the difference between 'vwn' and 'vwn,es' is small enough (1.945-1.939=0.006 eV at $E_{\text{MAX}}^{\text{APW}}=3.0$ Ry; 1.982-1.969 = 0.013 eV at $E_{\text{MAX}}^{\text{APW}}=6.0$ Ry). Thus we do not need to use ESs for GaAs.

There are other cases where we have no clear explanations because kinds of factors can affects to results. In the case of "vwn,es", 1.945 eV (for $E_{\text{MAX}}^{\Sigma}=\text{'all'}$) changes to 1.903 eV for $E_{\text{MAX}}^{\Sigma}=3$ Ry.

Corresponding change in 'vwn' is from 1.939eV to 1.942 eV.

When we use 'pbe' as the assistance of numerical calculation (explained at the bottom of Sec.III A), result changes a little. The best value 2.002 eV (marked by *) show a little difference of 0.02 eV from that in 'vwn,es' of 1.982 eV (marked by *).

As a conclusion, except non-converging behavior on $E_{\text{MAX}}^{\text{APW}}$, it might be safer to estimate numerical errors as ~ 0.1 eV, based on the dependence on computational conditions.

5. Let us discuss other points for SiO₂c.

In this case, we see not a small dependence on E_{MAX}^{Σ} for 'vwn'; it changes from 10.38 eV at $E_{\text{MAX}}^{\Sigma}=3.0\text{Ry}$ (marked by **) to 11.16 eV for 'all' (REF). The difference 11.16-10.38=0.78 eV looks too large, much more than our target of numerical error ~ 0.1 eV. In 'vwn,es', corresponding values are 10.09 eV and 10.49 eV, respectively. We see that the difference 10.38-10.09 eV for $E_{\text{MAX}}^{\Sigma}=3.0\text{Ry}$ between 'vwn' and 'vwn,es' is relatively small. However, the difference becomes larger as 11.16-10.49 eV for $E_{\text{MAX}}^{\Sigma}=\text{'all'}$. This means that the difference comes from the high energy part of the matrix elements of ΔV^{xc} . Generally speaking, higher energy parts are less reliable numerically. Considering the fact of no MTOs in ES, we think 11.16 eV of REF is not so reliable.

As we see the above paragraph, it looks not easy to obtain convergence for E_{MAX}^{Σ} in this case. Thus we think that we need to introduce a restriction to have good numerical accuracy. For example, we may look for convergence for $E_{\text{MAX}}^{\Sigma}=3.0\text{Ry}$. In fact, at $E_{\text{MAX}}^{\Sigma}=3.0\text{Ry}$, the difference between 'vwn' and 'vwn,es' is relatively small, 10.38-10.09 eV. That is, we can calculate the QSGW band gap with the numerical error of ~ 0.3 eV for $E_{\text{MAX}}^{\Sigma}=3.0\text{Ry}$. (in this case, 10.38 eV accidentally gives good agreement with 'vwn,es' for $E_{\text{MAX}}^{\text{APW}}=6.0\text{Ry}$).

Note that the difference between 'vwn,es' and 'pbe,es'. It gives an extra numerical error of $\sim 0.1\text{eV}$.

As a summary, convergence behaviors for band gap are satisfactory (convergence within ~ 0.1 eV) except for $E_{\text{MAX}}^{\text{APW}}$ when we include ESs. This was not apparent in FP-LMTO-QSGW since we have no $E_{\text{MAX}}^{\text{APW}}$ (no APWs). This is a limitation of the current implementation due to the limited ability of the PMT method to describe high energy bands (overcompleteness problem of a basis set). In addition, we see dependence on E_{MAX}^{Σ} when we do not use ESs in the case of SiO₂c; including ESs is not convenient to treat system such as slab models. If we use $E_{\text{MAX}}^{\Sigma}=3.0\text{Ry}$, we have smaller difference ~ 0.3 eV from the case including ESs.

Considering the balance of computational efforts and accuracy, we think that "PMT-QSGW with $E_{\text{MAX}}^{\Sigma} =$

$E_{\text{MAX}}^{\text{APW}} = 3.0$ Ry without ESSs” or similar is useful for practical calculations. This is taken as an approximation to the exact results of the fundamental equation of QSGW.

It might be not so meaning to obtain fully converged results in QSGW, since it is inevitable for QSGW to give some differences from experimental values. In fact, QSGW tends to give a little too large band gaps^{12,22} even if it is accurately performed. For example, calculated value of 10.41 eV (vwn) for SiO₂c in Table IV is rather larger than the experimental value ~ 8.9 eV⁴⁷, thus not directly compared with experiments (Other QSGW calculation by Shaltat et al¹⁷ gives band gap 8.8 eV by QSGW for SiO₂c. The difference from our value of 10.41 eV may indicate numerical difficulty to have convergence). In cases, we need to correct this discrepancy from experiments empirically by a hybrid method such as $(1 - \alpha) \times \text{QSGW} + \alpha \times \text{LDA}$ as was used in Refs.23 and 48 when we like to have good agreement with experiments ($\alpha \sim 0.2$). Thus, from a practical point of view, it will be better to take the parameter α as a combined correction on the theoretical error and the numerical errors due to the approximation as ‘PMT-QSGW with $E_{\text{MAX}}^{\Sigma} = E_{\text{MAX}}^{\text{APW}} = 3.0$ Ry without ESSs’. Or we may need to invent a better fundamental equation to go beyond QSGW, which is numerically stable with keeping advantages of QSGW and give better correspondence with experiments.

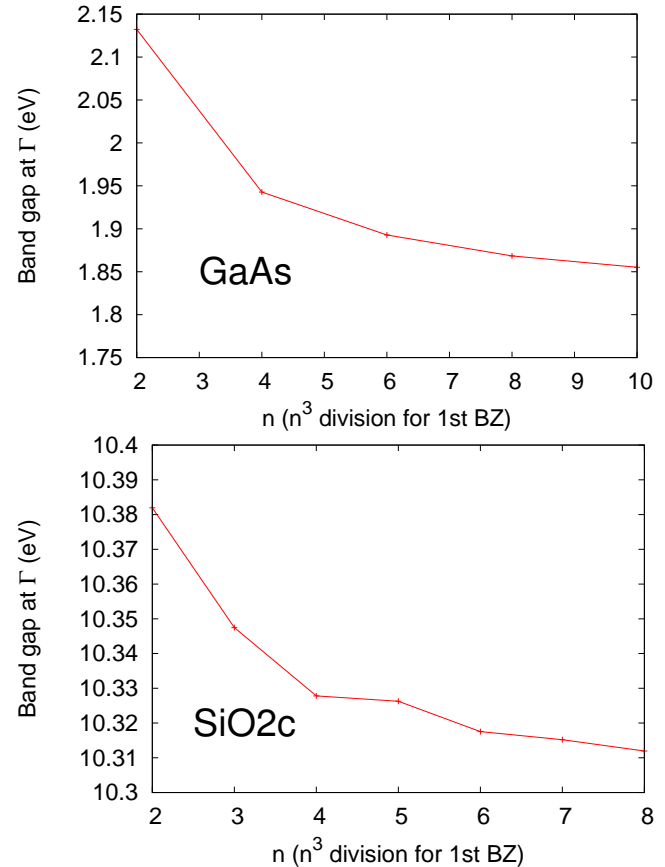
In Fig.1, we show the convergence check about the number of \mathbf{k} points for self-energy calculation in the 1st BZ (the \mathbf{k} point mesh for electron density is fixed). The integer n of x-axis means that the used number of \mathbf{k} points is $n \times n \times n$. As for GaAs, we see smooth convergence on the number of \mathbf{k} points. In the $4 \times 4 \times 4$ calculation, we see ~ 0.1 eV overestimation in comparison with the value at $10 \times 10 \times 10$. We need to choose number of \mathbf{k} points, to have best accuracy within the allowed computational resources. As for SiO₂c, pay attention to the energy scale of y-axis. The difference of the gap between $n = 2$ and $n = 8$ is rather small, only ~ 0.04 eV. In our analysis, unsmooth behavior of this plot is because of the cutoff of E_{MAX}^{Σ} ; see the dependence on E_{MAX}^{Σ} in Table.IV. Energy bands near E_{MAX}^{Σ} are taken into account or not by a slight change of \mathbf{k} point.

In Fig.2, the energy dispersion curve for QSGW obtained with the largest number of \mathbf{k} point cases in Fig.1 are shown, in order to show the difference from LDA/GGA.

V. SUMMARY

We have developed a new method, the PMT-QSGW method to perform the QSGW calculation based on the PMT method. PMT-QSGW have advantages in the robustness, easy to use, and accuracy in comparison with FP-LMTO-QSGW. We do not need to tune parameters for MTOs. Thanks to APWs, we can use highly local-

FIG. 1. Dependence of the band gap as for the number of \mathbf{k} points in the 1st BZ for self-energy calculation. Integer n of x-axis means the number of division of BZ is $n \times n \times n$. y-axis means the band gap.



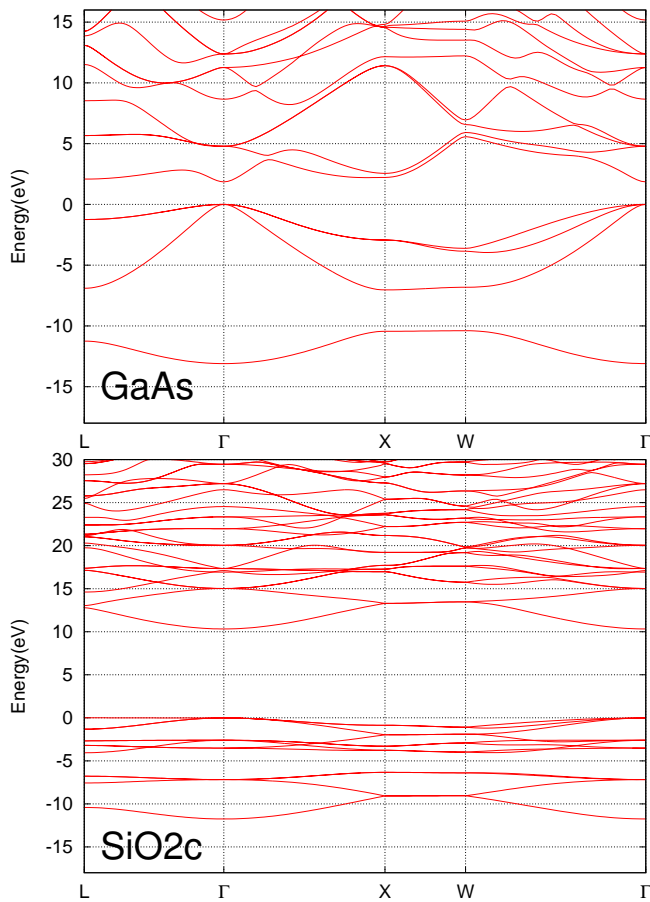
ized MTOs with low energy APWs (~ 4 Ry). Then we employ simplified interpolation procedure to the static component of the self-energy instead of previous complicated one in FP-LMTO-QSGW.

We have shown detailed convergence check on the band gaps of two typical cases, GaAs and cubic SiO₂. We analyzed how their band gaps depend on the cutoff parameters and computational settings. Then we see the performance and limitations of PMT-QSGW. We suggest ‘PMT-QSGW with $E_{\text{MAX}}^{\Sigma} = E_{\text{MAX}}^{\text{APW}} = 3.0$ Ry without ESSs’ as an approximation for practical usage. Results shown in this paper can be reproduced by the PMT-QSGW method implemented in the `ecalj` package, which is freely available from github⁴⁹.

The PMT-QSGW method with the highly localized MTOs and low energy APWs is advantageous for theoretical treatment. Techniques developed here can be useful even to go beyond QSGW.

Acknowledgement:

FIG. 2. Band plot for GaAs, corresponding to the case of $10 \times 10 \times 10$ in Fig.1, and for SiO₂c to the case of $8 \times 8 \times 8$.



I thank to Dr.H.Kino for discussions, codings, and advises to this manuscript. This work was partly supported by Advanced Low Carbon Technology Research and Development Program (ALCA) of Japan Science and Technology Agency (JST), and by Grant-in-Aid for Scientific Research 23104510. We also acknowledge computing time provided by Computing System for Research in Kyushu University.

- ¹ B. Holm and U. v. Barth, Phys. Rev. B **57**, 2108 (1998).
- ² W. Ku and A. G. Eguiluz, Phys. Rev. Lett. **89**, 126401 (2002).
- ³ A. Stan, N. E. Dahlen, and R. v. Leeuwen, Europhysics Letters (EPL) **76**, 298 (2006).
- ⁴ C. Rostgaard, K. W. Jacobsen, and K. S. Thygesen, Phys. Rev. B **81**, 085103 (2010).
- ⁵ F. Caruso, P. Rinke, X. Ren, A. Rubio, and M. Scheffler, Phys. Rev. B **88**, 075105 (2013).
- ⁶ S. V. Faleev, M. v. Schilfgaarde, and T. Kotani, Phys. Rev. Lett. **93**, 126406 (2004).
- ⁷ M. Methfessel, M. van Schilfgaarde, and R. A. Casali, in *Lecture Notes in Physics*, Vol. 535, edited by H. Dreyse (Springer-Verlag, Berlin, 2000).
- ⁸ T. Kotani and M. v. Schilfgaarde, Solid State Commun. **121**, 461 (2002).
- ⁹ F. Aryasetiawan and O. Gunnarsson, Phys. Rev. Lett. **74**, 3221 (1994).
- ¹⁰ F. Aryasetiawan and O. Gunnarsson, Phys. Rev. B **49**, 16214 (1994).
- ¹¹ F. Aryasetiawan and O. Gunnarsson, Rep. Prog. Phys **61**, 237 (1998).
- ¹² M. van Schilfgaarde, T. Kotani, and S. Faleev, Phys. Rev. Lett. **96**, 226402 (2006).
- ¹³ T. Kotani, M. van Schilfgaarde, and S. V. Faleev, Physical Review B **76**, 165106 (2007).
- ¹⁴ Adapting QSGW to large multi-core systems.
- ¹⁵ D. R. Hamann and D. Vanderbilt, Phys. Rev. B **79**, 045109 (2009).
- ¹⁶ M. Shishkin, M. Marsman, and G. Kresse, Physical Review Letters **99** (2007), 10.1103/PhysRevLett.99.246403.
- ¹⁷ R. Shaltaf, G.-M. Rignanese, X. Gonze, F. Giustino, and A. Pasquarello, Physical Review Letters **100**, 186401 (2008).
- ¹⁸ F. Bruneval, Physical Review Letters **103** (2009), 10.1103/PhysRevLett.103.186401.
- ¹⁹ F. Bruneval, The Journal of Chemical Physics **136**, 194107 (2012).
- ²⁰ S.-H. Ke, Phys. Rev. B **84**, 205415 (2011).
- ²¹ M. v. Schilfgaarde, T. Kotani, and S. V. Faleev, Phys. Rev. B **74**, 245125 (2006).
- ²² T. Kotani and M. van Schilfgaarde, Physical Review B **76** (2007), 10.1103/PhysRevB.76.165106, WOS:000250620600028.
- ²³ A. N. Chantis, M. v. Schilfgaarde, and T. Kotani, Phys. Rev. Lett. **96**, 086405 (2006).
- ²⁴ P. Lukashev, W. R. L. Lambrecht, T. Kotani, and M. van Schilfgaarde,

- Physical Review B (Condensed Matter and Materials Physics) **76**, 195202 (2007).
- ²⁵ T. Kotani and H. Kino, *Journal of Physics: Condensed Matter* **21**, 266002 (2009).
- ²⁶ N. E. Christensen, A. Svane, R. Laskowski, B. Palanivel, P. Modak, A. N. Chantisi, M. van Schilfgaarde, and T. Kotani, *Physical Review B* **81** (2010), 10.1103/PhysRevB.81.045203.
- ²⁷ A. Svane, N. E. Christensen, I. Gorczyca, M. van Schilfgaarde, A. N. Chantisi, and T. Kotani, *Physical Review B* **82** (2010), 10.1103/PhysRevB.82.115102.
- ²⁸ L.-y. Huang and W. R. L. Lambrecht, *Physical Review B* **88** (2013), 10.1103/PhysRevB.88.165203.
- ²⁹ T. Kotani and M. van Schilfgaarde, *Physical Review B* **81** (2010), 10.1103/PhysRevB.81.125117, WOS:000276248900054.
- ³⁰ T. Kotani and H. Kino, *Journal of the Physical Society of Japan* **82**, 124714 (2013).
- ³¹ I. V. Solovyev, A. I. Liechtenstein, and K. Terakura, *Phys. Rev. Lett.* **80**, 5758 (1998).
- ³² S. Ishii, H. Maebashi, and Y. Takada, arXiv , 1003.3342 (2000).
- ³³ B. Arnaud and M. Alouani, *Physical Review B* **63** (2001), 10.1103/PhysRevB.63.085208.
- ³⁴ F. Bechstedt, K. Tenelsen, B. Adolph, and R. D. Sole, *Phys. Rev. Lett.* **78**, 1528 (1997).
- ³⁵ S. Botti and M. A. L. Marques, *Physical Review Letters* **110** (2013), 10.1103/PhysRevLett.110.23401.
- ³⁶ X. Deng, M. Ferrero, J. Mravlje, M. Aichhorn, and A. Georges, *Physical Review B* **85** (2012), 10.1103/PhysRevB.85.125137.
- ³⁷ M. Springer, F. Aryasetiawan, and K. Karlsson, *Physical review letters* **80**, 2389 (1998).
- ³⁸ A. Georges, G. Kotliar, W. Krauth, and M. J. Rozenberg, *Rev. Mod. Phys.* **68**, 13 (1996).
- ³⁹ A. J. Cohen, P. Mori-Sanchez, and W. Yang, *Science* **321**, 792 (2008).
- ⁴⁰ C. Friedrich, S. Blgel, and A. Schindlmayr, *Physical Review B* **81** (2010), 10.1103/PhysRevB.81.125102.
- ⁴¹ J. Rath and A. J. Freeman, *Phys. Rev. B* **11**, 2109 (1975).
- ⁴² C. Freysoldt, P. Eggert, P. Rinke, A. Schindlmayr, R. Godby, and M. Scheffler, *Computer Physics Communications* **176**, 1 (2007).
- ⁴³ D. J. S. E. Sjostedt, L. Nordstrom, *Solid State Communications* **114**, 15 (2000).
- ⁴⁴ L. W. S. H. Vosko and M. Nusair, *Can. J. Phys.* **58**, 1200 (1980).
- ⁴⁵ J. P. Perdew, K. Burke, and M. Ernzerhof, *Phys. Rev. Lett.* **77**, 3865 (1996).
- ⁴⁶ C. Friedrich, M. C. Miller, and S. Blgel, *Phys. Rev. B* **83**, 081101 (2011).
- ⁴⁷ T. DiStefano and D. Eastman, *Solid State Communications* **9**, 2259 (1971).
- ⁴⁸ T. Kotani and M. van Schilfgaarde, *Physical Review B* **81** (2010), 10.1103/PhysRevB.81.125201.
- ⁴⁹ The first-principles electronic structure suite based on the `FP-LMTO` method, `ecalj` package, is freely available from <http://gh.codehum.com/tkotani/ecalj>.